Mutagenesis Advance Access published October 14, 2008
Mutagenesis pp. 1–9, 2008 doi:10.1093/mutage/gen057

Automated image analysis of cytokinesis-blocked micronuclei: an adapted protocol and a validated scoring procedure for biomonitoring

Ilse Decordier*, Alexander Papine[1], Gina Plas, Sam Roesems, Kim Vande Loock, Jennifer Moreno-Palomo[2], Eduardo Cemeli[3], Diana Anderson[3], Aleksandra Fucic[4], Ricardo Marcos[2], Françoise Soussaline[1] and Micheline Kirsch-Volders

Laboratorium voor Cellulaire Genetica, Vrije Universiteit Brussel, Pleinlaan 2, 1050 Brussels, Belgium, [1]IMSTAR, 60, rue Notre Dame des Champs, 75006 Paris, France, [2]Grup de Mutagènesi, Departament de Genètica i de Microbiologia, Universitat Autònoma de Barcelona, Bellaterra, Spain, [3]Department of Biomedical Sciences, University of Bradford, Bradford BD7 1DP, UK and [4]Institute for Medical Research and Occupational Health, 10000 Zagreb, Ksaverska c2, Croatia

Micronuclei (MN) frequencies in peripheral blood lymphocytes have been used worldwide as a biomarker of chromosomal damage for genotoxicity testing and biomonitoring studies. Automation of MN analysis would provide faster and more reliable results with minimizing subjective MN identification. We developed an automated facility for the scoring of the *in vitro* MN cytokinesis-block assay for biomonitoring on Giemsa-stained slides, fulfilling the following criteria: applicable to the cytokinesis-block micronucleus methodology, discriminating between mono-, bi- and polynucleated cells, MN scoring according to HUMN scoring criteria, false-negative MN rate <10% and false-positive (FP) MN rate <1%. We first adapted the slide preparation protocol to obtain an optimal cell density and dispersion, which is important for image analysis. We developed specific algorithms starting from the cell as a detection unit. The whole detection and scoring process was separated into two distinct steps: in the first step, the cells and nuclei are detected; then, in the second step, the MN are searched for in the detected cells. Since the rate of FP MN obtained by the automatic analysis was in the range of 0.5–1.5%, an interactive visual validation step was introduced, which is not time consuming and allows quality control. Validation of the automated scoring procedure was undertaken by comparing the results of visual and automated scoring of micronucleated mono- and binucleated cells in human lymphocytes induced by two clastogens (ionizing radiation and methyl methane-sulphonate), two aneugens (nocodazole and carbendazim) and one apoptogen (staurosporine). Although the absolute MN frequencies obtained with automated scoring were lower as compared to those detected by visual scoring, a clear dose response for MNBN frequencies was observed with the automated scoring system, indicating that it is able to produce biologically relevant and reliable results. These observations, together with its ability to detect cells, nuclei and MN in accordance with the HUMN scoring criteria, confirm the usability of the automated MN analysis system for biomonitoring.

Introduction

Analysis of micronucleus (MN) frequencies has since many years been applied for *in vitro* genotoxicity testing of new chemicals and for biomonitoring of human populations exposed to different environmental, occupational or lifestyle factors (1).

MN are found in interphase cells as small, extranuclear bodies resulting from chromosome breaks (leading to acentric fragments) and/or whole chromosomes that did not reach the spindle poles during cell division. At telophase, when the nuclear envelope is reconstituted around the two daughter cells, these lagging chromosomes or fragments are not incorporated into the main nucleus but encapsulated into a separate, smaller nucleus, a MN. MN represent therefore a measure of both chromosome breakage and chromosome loss and can be used to classify chemicals into clastogens or aneugens (2).

Since the formation of a MN requires a nuclear division, it is necessary to be able to distinguish dividing cells from resting cells. The cytokinesis-block micronucleus (CBMN) methodology developed by Fenech and Morley (3) uses cytochalasin B to identify cells that have divided in culture. Cytochalasin B is an inhibitor of actin polymerization which is required for the formation of the microfilament ring that constricts the cytoplasm between the daughter nuclei during cytokinesis (4). The CBMN methodology allows distinction between a mononucleated cell, that did not divide, and a binucleated cell that has divided once. micronuclei present in mononucleated cells (MNMONO) may provide an indication of the genome instability accumulated *in vivo*, while micronuclei in binucleated cells (MNBN) indicate the chromosome/genome mutations accumulated before cultivation plus lesions expressed during *in vitro* culture.

The International Collaborative Project on Micronucleus Frequency in Human Populations (the HUMN project, http://www.humn.org) established scoring criteria for MN using isolated human lymphocyte cultures and used combined databases to assess intra- and interlaboratory variation in MN scoring, background MN frequencies and the influence of culture conditions, age, gender and smoking on MN frequencies (5–10). In addition, a large international cohort study conducted within the frame of HUMN provided evidence that baseline frequency of MN in peripheral blood lymphocytes is a predictive biomarker of cancer risk (11,12).

Although the MN assay is well validated and easy to realize and to score, applicability on a large scale for environmental biomonitoring is hampered by lack of high-throughput technology. Visual scoring of MN can be very time consuming and large numbers of cells and/or donors have to be analysed to obtain statistically relevant data, especially for biomonitoring of populations characterized by low baseline MN frequencies such as children (13). Moreover, even under optimized laboratory conditions, often a high inter-scorer variation is

*To whom correspondence should be addressed. Tel: +32 2 629 34 28; Fax: +32 2 629 27 59; Email: idecordi@vub.ac.be

observed with visual MN analysis (9). Automation of the MN analysis is still a requirement and would provide a faster and more reliable analysis of MN frequencies with minimization of subjective identification of MN.

To obtain reliable results, an automated system for MN scoring used in biomonitoring studies should fulfil the same requirements as those for visual scoring: it should be applicable to the CBMN methodology and be able to perfectly distinguish mono-, bi- and polynucleated cells; furthermore, the detection of MN should be based on the scoring criteria described by the HUMN project. Up to now, only a few studies reported on the development of an automated image analysis system for the detection of MN. Castelain *et al*. (14) developed an algorithm to detect MN, which contained a sequence of grey operators and binary operators. However, this automated system still showed some limitations: errors occurred in the classification of binucleated cells due to overlapping nuclei and in the detection of some small MN. Moreover, it was developed at a time where no scoring criteria were yet available. More recently, Varga *et al*. (15) established an automated scoring procedure for the CBMN assay with algorithms to detect binucleated cells, with or without MN. A major drawback of this methodology is that binucleated cells were scored starting from two similar nuclei as detection unit and no information on cytoplasm was available.

In the present study, we describe an automated image analysis system for the scoring of the *in vitro* MN cytokinesis-block assay for biomonitoring on Giemsa-stained slides, applying all scoring criteria defined by the HUMN project and starting from the cell as a detection unit. For the latter, we developed specific algorithms which in a first step detected cells and nuclei, followed by a second step, in which the system searched for MN in the detected cells. In this context, we adapted the slide preparation protocol to obtain an optimal density and dispersion of the cells, which is of major importance for image analysis. Moreover, a standardized slide preparation protocol ensures a high reproducibility when large numbers of samples have to be prepared in parallel, which is the case for biomonitoring. To validate the automated scoring procedure, we compared the MN frequencies obtained by visual and automated scoring in human peripheral blood mononucleated cells (PBMC) treated with two clastogens: ionizing radiation (IR) and methyl methane-sulphonate (MMS), two aneugens: nocodazole (NOC) and carbendazim (CAR) and one apoptogen: staurosporine (STP).

The development of this automated facility for the scoring of the *in vitro* MN cytokinesis-block assay for biomonitoring was performed in the framework of the EU Integrated Project NewGeneris. This research project aims at investigating the role of prenatal and early-life exposure to genotoxic chemicals present in food and environment in the development of childhood cancer and immune disorders. Our contribution to this project is (i) to study the interaction between dietary carcinogens having also genotoxic and immunotoxic properties and the induction of MN as a validated biomarker for early mutagenic effects and (ii) to compare mother versus child genotoxic responses to a similar diet and environment using this biomarker.

Materials and methods

Preparation of slides suitable for automated image analysis of the CBMN assay for biomonitoring

Blood cultures Human blood samples from a healthy donor of 30-year old were drawn by venipuncture into heparinized tubes (Vacutainer; Becton Dickinson, Oxford, UK). Whole blood cultures (5 ml) were set up in RPMI1640/HEPES medium (Gibco BRL, Paisley, UK) supplemented with 15% foetal calf serum (Gibco BRL), 1% penicillin–streptomycin (Gibco BRL), 1% L-glutamine (Gibco BRL), 2% phytohaemagglutinin (PHA; Remel, Dartford, UK) and 7.5% whole blood and cultivated at 37°C. After 44 h, cytochalasin-B (Sigma-Aldrich, Steinheim, Germany) was added at a final concentration of 6 μg/ml.

Drug treatment of the blood cultures After 24 h PHA stimulation, the whole-blood cultures were treated with three concentrations and a concurrent control of the different mutagens (one culture per concentration). The choice of the concentrations was based on previous studies from the laboratory—for NOC (Acros Organics, Geel, Belgium): 0.01, 0.02 and 0.04 μg/ml (16); for CAR (Aldrich Chemie, Steinheim, Germany): 2.5, 5.0 and 7.5 μg/ml (16); for MMS (Sigma-Aldrich): 10, 20 and 30 μg/ml (16); for STP (Sigma-Aldrich): 0.029, 0.058 and 0.116 μg/ml (17) and for IR: 1, 2 and 3 Gy produced from a 60 Co source (18). NOC, CAR and STP were dissolved in dimethylsulphoxide (DMSO; Merck, Darmstadt, Germany) and MMS in phosphate-buffered saline (PBS). The control cultures were treated with the solvents of the mutagens: DMSO for NOC, CAR and STP and PBS for MMS. The final concentration of DMSO did not exceed 0.5%.

Hypotonic shock At 72 h, the whole-blood cultures were harvested and cells were centrifuged at 800 r.p.m./8 min at room temperature. After discarding the supernatant with water pump until 500 μl remained, cells were re-suspended by patting. Prior to fixation, cells were subjected to a cold hypotonic treatment at several KCl concentration: 75, 90, 100, 110, 125 and 140 mM and three hypotonic treatment times: 15, 30 and 45 min and were tested on untreated cell cultures. KCl was added on vortex (800 l/min) and cells were incubated at 4°C during the three tested times.

Fixation After hypotonic treatment, cells were centrifuged at 800 r.p.m./8 min at room temperature and fixed with 5 ml of 3:1 freshly prepared methanol/acetic acid which was added drop by drop on vortex (800 l/min), followed by three additional drops of formaldehyde. After centrifugation at 800 r.p.m./8 min at room temperature, the fixation was repeated twice without formaldehyde. After each centrifugation, the supernatant was discarded by water pump until 500 μl remained and cells were re-suspended by patting. After the last centrifugation, the supernatant was discarded until 100 μl remained and cells were re-suspended in 200–600 μl methanol/acetic acid, according to cell density.

Slide preparation The fixed cells were dropped, 2 × 20 μl, on dry slides using a micropipette on pre-marked positions, 13 mm from edges and frosted end, resulting in two clear separated spots. Two slides per culture were prepared, and slides were dried overnight.

Staining Slides were stained for 20 min in freshly prepared 5% Giemsa in Sörensen buffer (pH 6.8) (Prosan, Merelbeke, Belgium), which was filtered twice through Whatman 41 filter (Whatman International Ltd, Maidstone, UK).

Visual scoring At least 1000 binucleated cells were scored on one slide per concentration of the different mutagens for the presence of one, two or more MN and expressed per thousand (MNBN). The scoring criteria [http://www.humn.org (1,10)] for MN included round or oval shaped MN with no connection to the main nuclei, a size between 1/16 and 1/3 and similar staining characteristics of the main nuclei. In addition, the percentage of BN, polynucleated cells and mononucleated cells (MONO) with micronuclei (MNMONO) or without were scored. The slides were coded and analysed on a Zeiss transmitted light microscope at a magnification of ×400. From the data of the MN analysis, the cytokinesis-block proliferation index (CBPI) was calculated as follows: CBPI = (number of mononucleated cells + 2 × number of binucleated cells + 3 × number of polynucleated cells)/total number of cells.

PathFinder™ platform: high-content image cytometer for automated analysis of the CBMN assay

The PathFinder™ platform installed at the laboratory of Cell Genetics consists of a PathFinder™ CELLSCAN™ capture station and two PathFinder™ MN analysis workstations. This configuration fulfils the requirement of the EU Integrated Project NewGeneris to process up to 12 slides/day, while scoring a minimum of 2500 cells per slide, to ensure statistics of at least 1000 binucleated cells, and limiting the human intervention time to <1–2 min per slide.

The pathfinder™ CELLSCAN™ capture station The capture station comprises an upright microscope (Nikon E50i) equipped for bright field and fluorescence

with ×2, ×10, ×20, ×40 and ×100 objectives; motorized X-Y-Z stage (ProScan™, Prior) with four-slide holder; an opto-electronic device for multi-plan colour capture (BrightColor™, Imstar); a digital monochrome camera (C8484, Hamamatsu) with 1280 × 1024 resolution and 12 bits digitalization and a Windows XP Pro™ computer with Pathfinder™ software platform, including the following components: (i) Smart Capture Drivers for control of motorized components and camera; (ii) Pathfinder™ LightVision™ for automated slide scanning and capture in brightfield; (iii) Pathfinder™ CELLSCAN™ for cells, nuclei and MN detection and multiparametric results table output, presentation, validation and export and (iv) Pathfinder™ Batch Processor for the processing tasks distribution over the available processors (analysis workstations).

The pathfinder™ MN analysis workstation The MN analysis workstation consists of a Windows XP Pro™ computer with a Pathfinder™ software platform including the CELLSCAN™ module.

Automated analysis procedure The procedure of automated MN slide analysis as performed by the Pathfinder™ platform includes the following steps: (i) automated multiple-slide scanning and images capture; (ii) automated cells, nuclei and MN detection; (iii) optional validation of detected MNs by the user/expert and (iv) numerical results (scoring) reporting and export.

After the slides have been loaded in the holder, the following workflow is performed, slide by slide:

(i) The predefined scanning zone, corresponding to the pre-marked two-drop positions, is loaded. The software allows the user to modify the zone, this feature not being used in routine scoring, where the goal is to minimize the user interactions.
(ii) Landmarks for the automated focusing are set: this procedure consists of taking tens of images at different focus positions and choosing the one corresponding to the optimum focus. This procedure is too long to be applied to every field of view to be captured. Thus, the automatic focusing is performed on a limited set (usually 5) of positions within the zone to scan and subsequent focus positions are calculated by interpolation based on these five positions.
(iii) The zone is scanned (time of the order of 15 min), so that every field of view inside the zone is placed under the nosepiece, captured with ×10 objective by the camera and saved in a file including image and capture conditions. The ×10 magnification has been used for the performance reasons. The nuclei we detected are >10 μm in diameter, which, given the camera pixel size of 6.5 μm, corresponds to 16 image pixels. Thus, the MN to detect (given the HUMN criteria of theoretical minimum of 1/16 of the mean diameter of the main nuclei) exceed the image pixel size and thus are detectable. The real MN were actually resolved as >6 pixel objects because the diffraction limit of the ×10 objective is higher than the pixel size (Rayleigh criterion of 0.6 × wavelength/numerical aperture (NA) gives the resolution limit of ∼1 μM, for the 500 nm light and ×10 nosepiece with NA 0.3, which means that the object edges are >1 pixel).
(iv) When the slide scanning is completed, the slide images are queued for processing.
(v) The processing is started as soon as a Pathfinder™ Batch Processor is available (i.e. terminated the previous task) on one of the analysis stations.
(vi) At the end of processing, the user can ask for interactive validation: the cells containing detected MN are presented one by one; the user either confirms or rejects each MN individually.
(vii) After the validation, the results are exported to the preset file, in the format readable by spreadsheet or statistical analysis applications. The results include total numbers of mono-, bi-, tri- and polynucleated cells and number of cells of each type with one or more MN. In addition, the CBPI is calculated and presented in the results table.

Specific algorithms for the detection of the cells, nuclei and MN Cell and nuclei detection (see supplementary material, available at *Mutagenesis* Online):

(i) The cytoplasm regions are detected: optical density (OD) threshold is automatically set based on the parameters of the main peak of OD distribution in the image. Individual cells, cell clusters and various artefacts are detected at this step.
(ii) The nuclei regions are detected inside these cytoplasm regions. A threshold is set using the global analysis of the OD distribution, optimizing the detection of the convex objects separately for each cytoplasm region.
(iii) The separation of touching cells is performed, avoiding cuts through the nuclear regions. Thus, the cytoplasm regions corresponding to the cell clusters are separated into individual cells.
(iv) The nuclei are then detected inside the nuclei regions. They are then filtered according to their shape, relative size and texture. Most of the artefacts are thus eliminated.

Finally, the cells are filtered according to criteria of shape, size and number of nuclei (cytoplasm regions without detected nuclei or of atypical cell morphology are eliminated).

MN detection (see supplementary material, available at Mutagenesis Online):

(i) Large background variations are eliminated from the image.
(ii) The MN candidates are detected by OD thresholding as described above for cytoplasm regions detection.
(iii) The candidates MN are, then, filtered according to the following criteria:

(a) Size relative to the nuclei (MN/nucleus size ratio) in the given cell.
(b) Position within the cell: candidates touching the cell contour are discarded.
(c) Colour: candidates having a colour too different from the nuclei, such as dust particles, are removed.
(d) Circular symmetry: the MN candidates below a level of circular symmetry are removed.
(e) Local contrast: not sufficiently contrasted candidates are removed, the contrast being measured as the ratio of the candidate's OD to the OD of a cytoplasm ring around it.

Results

Slide preparation

For image analysis, it is important to standardize the slide preparation as much as possible to be able to analyse the images in an unambiguous and consistent way and to obtain an optimal reproducibility. Therefore, we first standardized the slide preparation protocol in order to obtain an optimal density and dispersion of the cells (Figure 1), avoiding overlapping of the cells, which is of major importance for image analysis to reach the most appropriate detection as possible. An important step in the slide preparation protocol is the hypotonic treatment which induces swelling of the cells and hence influences the

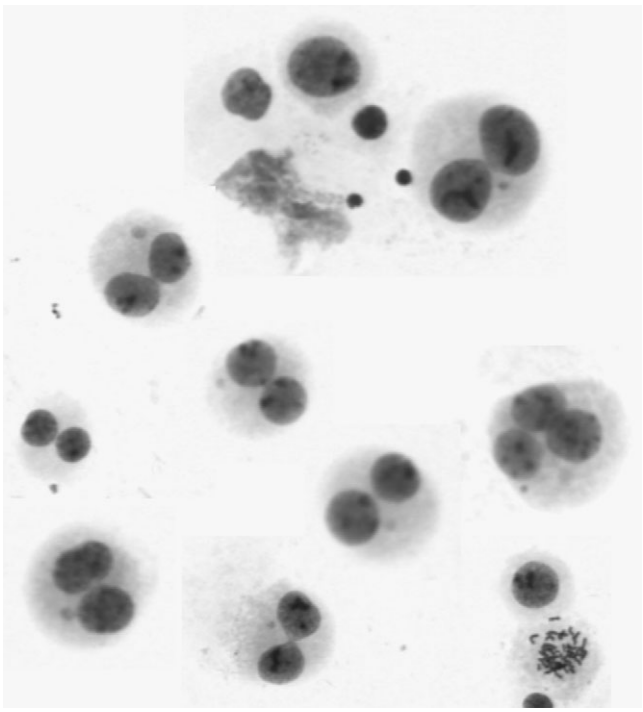

Fig. 1. Image of a suitable dispersion and swelling of cells for automated scoring. Cells are well dispersed and not overlapping.

detection of cells. Various concentrations of the hypotonic treatment (KCl), all applied at 4°C, were tested on untreated lymphocyte cultures to find the optimal detection which is not sensitive to small variations over the hypotonic exposure times. Figure 2 presents the total number of cells detected (Figure 2A) and the distribution of the different sub-populations (mono-, bi- and polynucleated cells) (Figure 2B), with the different KCl concentrations (75, 90, 100, 110, 125 and 140 mM) and times of hypotonic treatment (15, 30 and 45 min). At 140 mM of KCl, the lowest variation in the distribution of the sub-populations of cells was observed over the different times of hypotonic treatment, indicating that the duration of the hypotonic treatment did not have a major influence. However, in regard to the total number of cells detected, a hypotonic treatment of 110 mM showed the best detection capacity at 15 and 30 min. Since this KCl concentration of 110 mM also showed a consistent repartition of the sub-populations at 15 and 30 min, it was decided to apply this concentration of hypotonic treatment for 15 min at 4°C.

Besides changes to the hypotonic treatment, a few other steps in the slide preparation protocol were slightly adapted. To obtain an optimal spreading of the cells, without overlapping too much, the cells were re-suspended in a higher volume of fixative as compared to that used for the standard protocol before spreading onto slides.

Slides were stained with 5% Giemsa (14) instead of 10 % (19), in Sörensen buffer, to obtain an optimal contrast between nuclei and cells. Giemsa solution was freshly prepared and filtered twice to avoid artefacts in the detection due to debris present in the Giemsa solution (data not shown).

Validation of automated MN scoring by image analysis

To validate the image analysis system for the automated scoring of MN, we compared the results of automated and visual scoring of MN induced by two aneugens, NOC and CAR, showing a threshold in dose response; two clastogens, IR and MMS, without threshold in dose response, and a non-genotoxic apoptogen, STP. The latter was included to verify

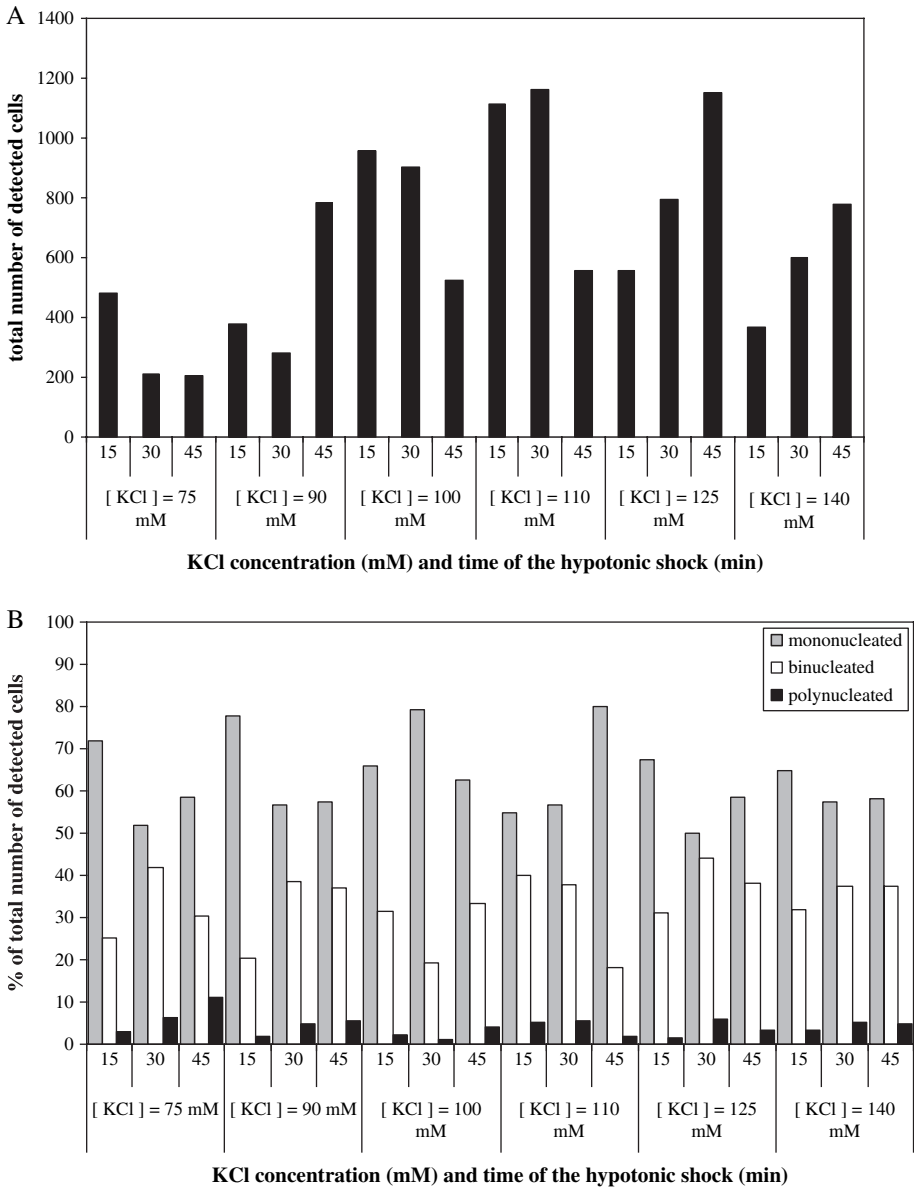

Fig. 2. (**A**) Total number of cells detected in function of KCl concentration and time of hypotonic treatment. (**B**) Distribution of the different sub-populations (mono-, bi- and polynucleated cells) in function of KCl concentration and time of hypotonic treatment.

whether the automated analysis system was able to discriminate between MN and apoptotic bodies. For each compound, three concentrations and corresponding controls were analysed. The visual scoring was performed by an experienced scorer (G). As performed with visual scoring, the automated image analysis system detected mono-, bi- and polynucleated cells allowing to calculate the CBPI, and MN were scored in mononucleated (MNMONO) and binucleated (MNBN) cells. The frequencies of these micronucleated cells and CBPI were compared between the two scoring methods, for which the same coded slides were used. Table I presents an overview of the total number of cells, percentage of mononucleated, binucleated and polynucleated cells detected by visual scoring and by automated scoring, and the CBPI calculated from these values for the two scoring methods. When comparing the CBPI for the five compounds tested, very similar values were obtained with the two scoring procedures.

Since the rate of false-positive (FP) MN obtained by the automatic analysis was in the range of 0.5–1.5% (data not shown), an interactive visual validation step was introduced. MN scored by the automatic detection are presented one by one on the screen (Figure 3), the scorer has to either validate or invalidate (=FP) the MN found by the automated analysis. It is also possible to label it for future review in case of doubt. This interactive validation step was performed by the same scorer (G) who performed the visual scoring.

Table II presents the comparison of MN frequencies in mono- and binucleated cells (MNBN and MNMONO) obtained by visual, automated and automated scoring after visual validation. Comparison of the MN frequencies between automated and automated scoring after visual validation showed that the visual validation step is required to reduce the FP MN. Nevertheless, comparison of the frequencies of MNBN obtained by visual and automated scoring after visual validation for the five compounds tested shows that both scoring methods detect a dose response for the two clastogens and aneugens analysed. However, in all cases, lower frequencies of MNBN were detected with the automated system as compared to the visual scoring. As far as the frequencies of MNMONO are concerned, with both visual and automated scoring with visual validation, a clear increase was observed for the highest dose of NOC and CAR, which is expected from aneugens inducing mitotic slippage at high concentrations. Again, lower MN frequencies were found with the automated scoring with visual validation as compared to the visual scoring. For MMS and IR, as expected from clastogens, no increase in the frequencies of MNMONO was observed, neither with visual nor with automated scoring. Concerning the apoptogen STP, as expected no significant increase in MN was observed, neither in mononucleated nor in binucleated cells, with both scoring methods.

In order to investigate the reproducibility of the automated image analysis combined with the visual validation step, we assessed its inter-capturing variability. Therefore, the same coded slides used for the comparison between visual and automated scoring with visual validation were captured and analysed four more times and visually validated by the same scorer (G), i.e. all slides were scored five times. With the four additional capturing sessions, the results were similar to the first capture session (Figure 4). A dose response in MNBN

Table I. Comparison of total number of cells, percentage of mononucleated, binucleated, and polynucleated cells detected by visual scoring (vis) and by automated scoring (auto) and the CBPI calculated from these values for the two scoring methods

	Total number of cells		% Mononucleated cells		% Binucleated cells		% Polynucleated cells		CBPI	
	vis	auto	vis	auto	vis	auto	vis	auto	vis	auto
MMS										
Untreated	1000	5184	29.0	45.8	61.4	50.1	9.6	4.1	1.8	1.6
PBS	1000	4826	36.2	32.1	57.2	63.8	6.6	4.1	1.7	1.7
10 μg/ml	1000	5091	48.0	47.0	48.4	50.9	3.6	2.1	1.6	1.6
20 μg/ml	1000	3974	49.2	61.5	48.0	37.5	2.8	1.0	1.5	1.4
30 μg/ml	1000	1514	69.8	72.6	29.6	27.0	0.6	0.4	1.3	1.3
IR										
Untreated	1000	3860	35.8	49.6	52.0	43.2	12.2	7.2	1.6	1.6
1 Gy	1000	5760	33.2	58.7	61.8	38.9	5.0	2.4	1.7	1.4
2 Gy	1000	4127	58.4	69.7	39.8	29.2	1.8	1.1	1.4	1.3
3 Gy	1000	4647	71.7	79.1	26.3	20.1	2.0	0.9	1.3	1.2
NOC										
Untreated	1000	5184	29.0	45.8	61.4	50.1	9.6	4.1	1.6	1.6
DMSO	1000	4776	31.3	35.7	57.1	58.8	11.6	5.5	1.8	1.7
0.01 μg/ml	1000	3980	30.5	39.3	61.7	56.1	7.8	4.5	1.8	1.7
0.02 μg/ml	1000	4135	29.0	43.1	59.4	52.4	11.6	4.4	1.8	1.6
0.04 μg/ml	1000	4461	40.0	56.5	57.2	41.9	2.8	1.5	1.6	1.4
CAR										
Untreated	1000	5184	29.0	45.8	61.4	50.1	9.6	4.1	1.6	1.6
DMSO	1000	4776	31.3	35.7	57.1	58.8	11.6	5.5	1.8	1.7
2.5 μg/ml	1000	2865	34.2	36.1	57.3	58.8	8.5	5.0	1.7	1.7
5.0 μg/ml	1000	2286	35.2	34.2	55.2	61.5	9.6	4.2	1.7	1.7
7.5 μg/ml	1000	5928	38.6	37.2	56.4	60.3	5.0	2.5	1.7	1.7
STP										
Untreated	1000	5184	29.0	45.8	61.4	50.1	9.6	4.1	1.6	1.6
DMSO	1000	4776	31.3	35.7	57.1	58.8	11.6	5.5	1.8	1.7
0.029 μg/ml	1000	2211	39.6	26.9	54.3	71.0	6.1	2.1	1.7	1.8
0.058 μg/ml	1000	3397	38.4	35.7	55.2	61.6	6.4	2.6	1.7	1.7
0.116 μg/ml	1000	4034	43.4	29.7	51.3	67.9	5.3	2.4	1.6	1.7

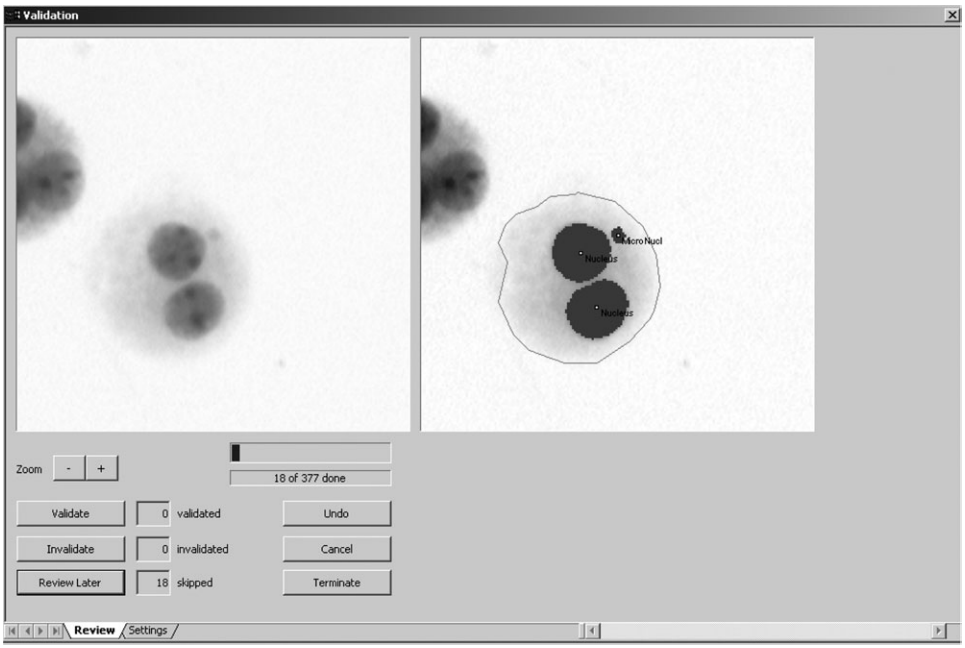

Fig. 3. Validation screen for the interactive visual validation step, MN detected by the automated system are presented one by one; for each MN, the scorer has to either validate it or invalidate it (=FP) or label it for future review.

Table II. Comparison of MN frequencies in bi- and mononucleated cells (MNBN and MNMONO) obtained by visual (vis), automated (auto) and automated scoring after manual validation (val)

	‰ MNBN			‰ MNMONO		
	vis	auto	val	vis	auto	val
MMS						
Untreated	4.0	21.9	3.8	0.0	13.1	2.2
PBS	5.0	20.1	3.2	1.6	27.8	2.0
10 µg/ml	10.0	14.7	8.1	0.0	2.2	0.0
20 µg/ml	21.0	28.6	19.1	0.0	9.8	0.0
30 µg/ml	47.0	41.6	26.9	0.0	2.6	0.0
IR						
Untreated	6.0	9.6	2.4	2.9	9.6	0.0
1 Gy	107.0	59.0	47.8	3.7	13.2	2.0
2 Gy	275.0	126.1	102.1	4.1	8.4	2.5
3 Gy	483.0	298.0	261.5	9.2	12.7	5.3
NOC						
Untreated	4.0	21.9	3.8	0.0	13.1	2.2
DMSO	5.8	12.5	3.6	1.8	16.4	1.6
0.01 µg/ml	5.0	15.7	3.6	2.0	18.6	1.4
0.02 µg/ml	7.0	14.3	5.1	2.0	25.5	6.1
0.04 µg/ml	53.0	39.0	19.2	50.1	48.2	18.5
CAR						
Untreated	4.0	21.9	3.8	0.0	13.1	2.2
DMSO	5.8	12.5	3.6	1.8	16.4	1.6
2.5 µg/ml	6.0	16.0	4.2	1.7	13.0	0.0
5.0 µg/ml	7.0	29.9	8.5	1.6	10.8	1.8
7.5 µg/ml	38.0	42.8	20.1	1.5	42.1	11.3
STP						
Untreated	4.0	21.9	3.8	0.0	13.1	2.2
DMSO	5.8	12.5	3.6	1.8	16.4	1.6
0.029 µg/ml	6.0	49.0	8.9	5.5	26.4	2.6
0.058 µg/ml	12.0	17.2	5.3	7.2	8.6	0.0
0.116 µg/ml	8.0	28.5	6.9	3.5	13.7	2.3

frequencies was found for the two clastogens (Figure 4A and B) and aneugens (Figure 4C and D) analysed, but lower frequencies of MN, both in binucleated (MNBN) and mononucleated (MNMONO) cells, as compared to the visual scoring. Furthermore, no difference in CBPI was observed for all compounds analysed (data not shown).

To investigate the inter-scorer variability of the visual validation procedure, a second independent scorer (S) performed the visual validation of the same five capturing sessions. Comparison of the results obtained by the two independent scorers is shown in Figure 4. The values obtained for MNBN and MNMONO frequencies by the five capturing sessions and the visual validation step performed by the two different scorers were highly correlated with those of the visual scoring for the two clastogens and aneugens studied, despite the differences in absolute MN frequencies (Table III).

Discussion

For many years, the CBMN assay has been successfully applied for human biomonitoring of *in vivo* genotoxin exposure and provides a sensitive and relatively easy methodology to assess mutations (1). Moreover, the fact that baseline MN frequencies in cytokinesis-blocked lymphocytes have been shown to be a predictive biomarker for cancer risk (11,12) strengthens the importance of the CBMN assay as a reliable methodology for human biomonitoring of early genetic effects. Nevertheless, there is need for automation of MN analysis for quicker and more reliable detection with minimizing subjective judgement and individual scoring skills. Additionally, for biomonitoring purposes, automation would increase the sensitivity, which is of major importance when low MN frequencies have to be detected. For this goal to be achieved, we decided that the following requirements should be fulfilled: the automated MN analysis system should be able to clearly detect and distinguish mono-, bi- and polynucleated cells; for MN scoring the same criteria should be applied as defined by HUMN; the false-negative MN rate (ratio of number of detected MN to number of all MN) should be 10% and the FP rate (ratio of number of cells without MN where MN has been

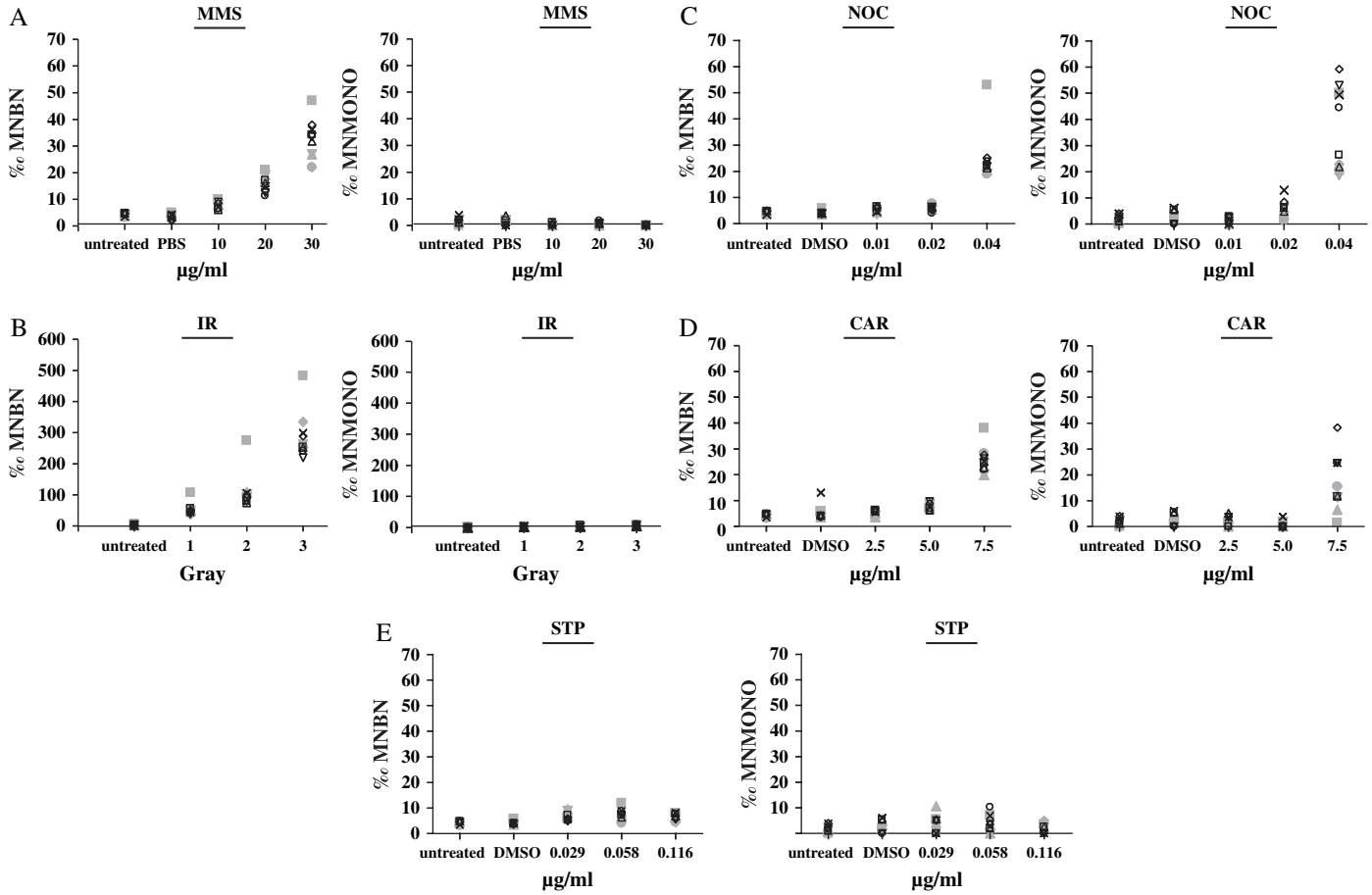

Fig. 4. Inter-capturing session and inter-scorer comparison for the frequencies of MNBN, MNMONO for MMS (**A**), IR (**B**), NOC (**C**), CAR (**D**) and STP (**E**). Five independent capturing sessions were performed. For the inter-scorer assessment two independent scorer (G and S) performed the visual validation of the same five capturing sessions (Auto G1-G5, Auto S1-S5). Filled squares, Man; filled triangles, Auto_S1; inverted filled triangles, Auto_G1; filled diamonds, Auto_S2; filled circles, Auto_G2; open squares, Auto_S3; open triangles, Auto_G3; open inverted triangles, Auto_S4; open diamonds, Auto_G4; open circles: Auto_S5 and cross, Auto_G5.

Table III. Linear correlation coefficient (*R*) between MNCB frequencies obtained with manual scoring and automated scoring for the five independent capturing sessions

	Session 1		Session 2		Session 3		Session 4		Session 5	
	Scorer G	Scorer S	Scorer G	Scorer S	Scorer G	Scorer S	Scorer G	Scorer S	Scorer G	Scorer S
MMS	0.962	0.963	0.963	0.952	0.995	0.996	0.990	0.988	0.999	0.987
IR	0.981	0.985	0.962	0.964	0.952	0.955	0.971	0.973	0.973	0.977
NOC	0.998	0.996	0.975	0.992	0.991	0.992	0.993	0.996	0.995	0.994
CAR	0.970	0.991	0.995	0.992	0.995	0.995	0.986	0.981	0.993	0.993
STP	0.140	0.178	0.206	0.321	0.616	0.628	0.895	0.913	0.896	0.852

detected to the total cell number) <1%. Furthermore, it should allow a faster and more efficient MN analysis and quality control. Developing an automated image analysis for the CBMN assay taking into account these considerations was only possible through an intensive collaboration between cytologists with a large experience in visual scoring and a high-technology company highly experienced in imaging automated systems, who could both understand the research question.

Compared to other automated image analysis systems to score MN described up to now (14,15), the automated scoring of MN developed in the present study provides several advantages and improvements:

(i) We first standardized the slide preparation protocol by adapting the hypotonic treatment in order to obtain uniformity in cell size, which is important when different laboratories are preparing slides that have to be analysed by the same image analysis system.

(ii) The software protocol that was developed for the automated scoring of MN started from the detection of cells and hence the identification of the cytoplasm, followed by the identification of the mono-, bi- and polynucleated cells, and MN in these different sub-populations of cells. We separated the whole detection and scoring process into two distinct steps: in the first step,

the cells and nuclei are detected; then, in the second step, the MN are searched for in the detected cells. The algorithms were applied to every individual image. The choice of the parameters for these algorithms was performed following an iterative process with important participation of the experienced visual scorers, who also participated in the MN studies of the HUMN project (9): the parameters were chosen to fit as closely as possible with the scorer's choice of viable cells, nuclei and MN to score. The scoring criteria were based on the HUMN programme [http://www.humn.org (1,9)]. To us, it was essential to start from the cell as detection unit, in order to obtain results on mono-, bi- and polynucleated cells and not to restrict to the analysis of binucleated cells. At first, information on these different cell classes allows the assessment of cell proliferation through nuclearity index, which is important for an efficient assessment of the genetic damage in human biomonitoring (1,6,20,21). At second, scoring of mononucleated cells also allows the detection of MN in those cells (MNMONO). Information on the frequencies of MNMONO may provide an indication of the genome instability accumulated *in vivo*, while MNBN indicate the chromosome/genome mutations accumulated *in vivo* before cultivation plus lesions expressed during *in vitro* culture. Moreover, micronucleated mononucleated cells can also constitute tetraploid mononucleated cells arising after mitotic slippage in presence of microtubule inhibitors. This is important to be taken into account when investigating the aneugenic potential of chemicals (reviewed in ref. 22). Besides the fact that the acquisition starting at cell level instead of nucleus level provides information on cell proliferation, it also provides the possibility to detect apoptotic and necrotic cells, nucleoplasmic bridges and nuclear buds (23).

(iii) The specific detection algorithms were developed to identify cells, nuclei and MN on Giemsa-stained slides. Giemsa staining has the advantage that the slides do not have to be protected from the light which allows a more efficient acquisition as compared to fluorescent dyes that need protection from light. Moreover, this staining also provides the advantage that the slides can be easily re-examined visually if necessary without loss of quality of the staining. In a study by Castelain *et al.* (14), an algorithm was developed to detect MN on Giemsa and Feulgen-Congo-Red-stained slides and also started from the cell as detection unit, allowing the detection of mono-, bi- and polynucleated cells. However, this system showed a misclassification of binucleated cells, mainly due to non-separation of overlapping nuclei. Although the authors compared different slide preparation procedures, no robust standardized protocol was established. In a more recent study by Varga *et al.* (15), an automated scoring procedure was developed for the CBMN assay, with algorithms developed to detect only binucleated cells, with or without MN, using two similar non-overlapping nuclei, as unit of detection, without acquiring information on nuclearity. Also in this study, a standardized slide preparation protocol was missing.

(iv) Comparison of MN frequencies in PBMC, exposed to five well-known mutagens, obtained by visual scoring to those obtained with automated scoring revealed that both scoring methods are able to detect a dose response.

(v) Comparison of the CBPI obtained from the visual and the automated scoring showed that the detection of the different sub-populations of cells (mono-, bi- and polynucleated cells) was very accurate.

(vi) By MN analysis in STP-treated cultures, we excluded that the detected micronucleated cells by the automated image system correspond to apoptotic bodies, thus confirming that the image analyser can distinguish MN from apoptotic bodies.

(vii) As far as the reproducibility is concerned, with the automated image analysis system presented here very similar results were obtained between different capturing sessions combined with the visual validation step. For each capturing and analysis session combined with the visual validation by two independent scorers, a clear dose response in MN frequencies was observed. In addition, MNBN frequencies found for the five capturing sessions and the visual validation step performed by the two different scorers were highly correlated with those of the visual scoring, indicating the ability of the automated scoring system to detect biological differences as observed by visual scoring.

Nevertheless, the automated image analysis system for MN detection described here also shows some limitations:

(i) Since the current FP rate was not always below the required 1%, we decided to include a visual validation step, which is performed visually on screen by a scorer. However, this human interaction is not time consuming, provides a good quality control and allows to re-analyse the same sample.

(ii) The MN frequencies obtained with the automated system were lower as compared to the visual scoring, and in particular, the automated system was less efficient in detecting high frequencies of MN at the highest concentrations of the two clastogens and aneugens tested. A similar phenomenon of a drop in MN frequencies detected with automated analysis as compared to visual scoring was also observed by Varga *et al.* (15) when analysing MN frequencies in lymphocytes of control and breast cancer patients. In that study, the differences between visual and automated scoring were larger as compared to our data: on average, only 34.5 % of the MN scored visually were detected by the automated system, while in the present study the mean detection rate was 68.5%. The automated MN detection system described by Castelain *et al.* (14) also missed a part of the MN detected visually; they found an overall detection rate of $\sim$51%. Nevertheless, it is difficult to directly compare our results on the accuracy of automated MN detection with these previously described studies, since different slide preparation protocols were used and low numbers of binucleated cells ($<$500) were analysed (14). In addition, visual and automated scoring was performed on different slides from the same cultures, stained with Giemsa and 4′, 6-diamidino-2-phenylindole (DAPI), respectively (15). There are several plausible explanations for the lower MN detection rate obtained with automated scoring described in the present study. The differences may in part be explained by the very strict scoring criteria that were applied for the automated image analysis. When MN detected by the automated system were doubtful according to the scorers performing the visual validation step, these MN were not labelled as valid MN. When performing the visual scoring using the direct microscope observation, the scorers, in the case of doubt, may slightly modify the focus, thus possibly validating

a doubtful object as MN. Furthermore, one can assume that the detection of MN, in particular small MN, is very close to the detection limit of the image analysis system. We verified whether the underestimation of small MN was not due to the capturing at a low magnification (×10). Therefore, some slides were captured with the ×20 objective and MN results were compared with those obtained with a capturing session performed with the ×10 objective (data not shown). Similar results were obtained with both magnifications, indicating that very small MN observed on a ×20 image are still visible on a ×10 image. Another plausible explanation for the lower MN frequencies found with the automated scoring as compared to visual scoring at the highest concentrations could be the irregular shape of nuclei. At those high mutagen concentrations, cells accumulate more genetic damage which often results in a higher number of MN per cell and more irregular nuclei. Nevertheless, with the automated system, the number of cells to be analysed can easily be increased (e.g. up to 5000 cells), thereby reducing the number of errors in the detection of MN. Moreover, we aimed at developing an automated image analysis system for MN scoring specifically for biomonitoring for which we do not expect very high MN frequencies.

In summary, in the present manuscript, we presented an automated image analysis system for the scoring of the *in vitro* MN cytokinesis-block assay for biomonitoring, starting from the cell as a unit for detection and developed a standardized slide preparation protocol suitable for automated scoring. The automated scoring application automatically scans slides, detects cells, nuclei and MN, following the HUMN scoring criteria. A visual validation of MN is still required, but provides an additional quality control which is limited to only a few minutes per slide. Although the absolute MN frequencies found with automated scoring were lower as compared to those obtained by visual scoring, the automated scoring system is able to produce biologically relevant and reliable results, with low inter-scorer variability in the visual validation step, and thus which can be used for biomonitoring. In the near future, we aim at further developing the automated scoring system for a more efficient detection of high MN frequencies; the detection of apoptosis/necrosis, nucleoplasmic bridges and nuclear buds, which would also allow its usability for *in vitro* genotoxicity testing.

Supplementary data

Supplementary material is available at *Mutagenesis* Online.

Funding

EU Integrated Project NewGeneris (acronym of the project 'Newborns and Genotoxic exposure risks' http://www.newgeneris.org), 6th Framework Programme, Priority 5: Food Quality and Safety (Contract no. FOOD-CT-2005-016320).

Acknowledgements

Conflict of interest statement: None declared

References

1. Fenech, M. (2007) Cytokinesis-block micronucleus cytome assay. *Nat. Protoc.*, **2**, 1084–1104.
2. Mateuca, R., Lombaert, N., Aka, P. V., Decordier, I. and Kirsch-Volders, M. (2006) Chromosomal changes: induction, detection methods and applicability in human biomonitoring. *Biochimie*, **88**, 1515–1531.
3. Fenech, M. and Morley, A. A. (1985) Measurement of micronuclei in lymphocytes. *Mutat. Res.*, **147**, 29–36.
4. Carter, S. B. (1967) Effects of cytochalasins on mammalian cells. *Nature*, **213**, 261–264.
5. Fenech, M. (1998) Chromosomal damage rate, aging, and diet. *Ann. N. Y. Acad. Sci.*, **854**, 23–36.
6. Fenech, M., Holland, N., Chang, W. P., Zeiger, E. and Bonassi, S. (1999) The human micronucleus project—an international collaborative study on the use of the micronucleus technique for measuring DNA damage in humans. *Mutat. Res.*, **428**, 271–283.
7. Bonassi, S., Fenech, M., Lando, C. *et al.* (2001) Human Micronucleus Project: international database comparison for results with the cytokinesis-block micronucleus assay in human lymphocytes: I. Effect of laboratory protocol, scoring criteria, and host factors on the frequency of micronuclei. *Environ. Mol. Mutagen.*, **37**, 31–45.
8. Bonassi, S., Neri, M., Lando, C. *et al.* (2000) Effect of smoking habit on the frequency of micronuclei in human lymphocytes: results from the human micronucleus project. *Mutat. Res.*, **543**, 155–166.
9. Fenech, M., Bonassi, S., Turner, J. *et al.* (2003) Intra- and inter-laboratory variation in the scoring of micronuclei and nucleoplasmic bridges in binucleated human lymphocytes. Results of an international slide-scoring exercise by the HUMN project. *Mutat. Res.*, **534**, 45–64.
10. Fenech, M., Chang, W. P., Kirsch-Volders, M., Holland, N., Bonassi, S. and Zeiger, E. and Human Micronnucleus Project (2003) HUMN project: detailed description of the scoring criteria for the cytokinesis-block micronucleus assay using isolated human lymphocyte cultures. *Mutat. Res.*, **534**, 65–75.
11. Bonassi, S., Znaor, A., Ceppi, M. *et al.* (2007) An increased micronucleus frequency in peripheral blood lymphocytes predicts the risk of cancer in humans. *Carcinogenesis*, **28**, 625–631.
12. Murgia, E., Ballardin, M., Bonassi, S., Rossi, A. M. and Barale, R. (2008) Validation of micronuclei frequency in peripheral blood lymphocytes as early cancer risk biomarker in a nested case-control study. *Mutat. Res.*, **39**, 27–34.
13. Neri, M., Ceppi, M., Knudsen, L. E., Merlo, D. F., Barale, R., Puntoni, R. and Bonassi, S. (2005) Baseline micronuclei frequency in children: estimates from meta- and pooled analyses. *Environ. Health Perspect.*, **113**, 1226–1229.
14. Castelain, P., Van Hummelen, P., Deleener, A. and Kirsch-Volders, M. (1993) Automated detection of cytochalasin-B blocked binucleated lymphocytes for scoring micronuclei. *Mutagenesis*, **8**, 285–293.
15. Varga, D., Johannes, T., Jainta, S., Schuster, S., Schwarz-Boeger, U., Kiechle, M., Patino Garcia, B. and Vogel, W. (2004) An automated scoring procedure for the micronucleus test by image analysis. *Mutagenesis*, **19**, 391–397.
16. Elhajouji, A., Tibaldi, F. and Kirsch-Volders, M. (1997) Indication for thresholds of chromosome non-disjunction versus chromosome lagging induced by spindle inhibitors in vitro in human lymphocytes. *Mutagenesis*, **12**, 133–140.
17. Decordier, I., Cundari, E. and Kirsch-Volders, M. (2005) Influence of caspase activity on micronuclei detection: a possible role for caspase-3 in micronucleation. *Mutagenesis*, **20**, 173–179.
18. Godderis, L., Aka, P., Mateuca, R., Kirsch-Volders, M., Lison, D. and Veulemans, H. (2006) Dose-dependent influence of genetic polymorphisms on DNA damage induced by styrene oxide, ethylene oxide and gamma-radiation. *Toxicology*, **219**, 220–229.
19. Lucero, L., Pastor, S., Suárez, S., Durbán, R., Gómez, C., Parrón, T., Creus, A. and Marcos, R. (2000) Cytogenetic biomonitoring of Spanish greenhouse workers exposed to pesticides: micronuclei analysis in peripheral blood lymphocytes and buccal epithelial cells. *Mutat. Res.*, **464**, 255–262.
20. Kirsch-Volders, M. and Fenech, M. (2001) Inclusion of micronuclei in non-divided mononuclear lymphocytes and necrosis/apoptosis may provide a more comprehensive cytokinesis block micronucleus assay for biomonitoring purposes. *Mutagenesis*, **16**, 51–58.
21. Kirsch-Volders, M., Sofuni, T., Aardema, M. *et al.* (2003) Report from the *in vitro* micronucleus assay working group. *Mutat. Res.*, **540**, 153–163.
22. Decordier, I., Cundari, E. and Kirsch-Volders, M. (2008) Survival of aneuploid, micronucleated and/or polyploid cells: crosstalk between ploidy control and apoptosis. *Mutat. Res.*, **651**, 30–39.
23. Fenech, M. (2006) Cytokinesis-block micronucleus assay evolves into a ''cytome'' assay of chromosomal instability, mitotic dysfunction and cell death. *Mutat. Res.*, **600**, 58–66.

Received on June 2, 2008; revised on September 17, 2008; accepted on September 18, 2008